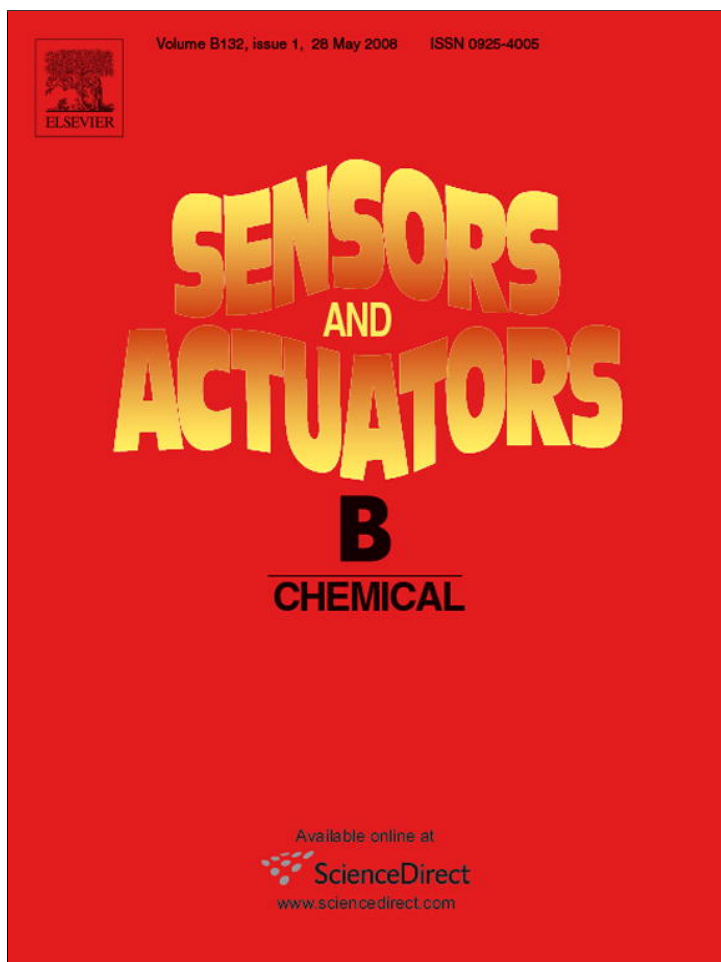


Provided for non-commercial research and education use.
Not for reproduction, distribution or commercial use.



This article appeared in a journal published by Elsevier. The attached copy is furnished to the author for internal non-commercial research and education use, including for instruction at the authors institution and sharing with colleagues.

Other uses, including reproduction and distribution, or selling or licensing copies, or posting to personal, institutional or third party websites are prohibited.

In most cases authors are permitted to post their version of the article (e.g. in Word or Tex form) to their personal website or institutional repository. Authors requiring further information regarding Elsevier's archiving and manuscript policies are encouraged to visit:

<http://www.elsevier.com/copyright>



Redox level-dependent impedance model for conjugated polymer actuators

Yang Fang^a, Xiaobo Tan^{a,*}, Gursel Alici^b

^a *Smart Microsystems Laboratory, Department of Electrical & Computer Engineering, Michigan State University, East Lansing, MI 48824, USA*

^b *School of Mechanical, Materials & Mechatronics Engineering, University of Wollongong, 2522 NSW, Australia*

Received 20 October 2007; accepted 14 January 2008

Available online 21 January 2008

Abstract

The reduction–oxidation (redox) level of a conjugated polymer has significant impact on its electro-chemo-mechanical properties, such as conductivity, impedance, and Young's modulus. Understanding and modeling the influence of redox level is of interest to both fundamental understanding of conjugated polymers and practical applications of these materials. In this paper a redox level-dependent impedance model is developed by incorporating dynamics of ionic diffusion, ionic migration, and redox reaction. The model, in the form of a transfer function, is derived through perturbation analysis around a given redox level, and extends the diffusive-elastic-metal model proposed by J. Madden. Experimental measurements under various redox conditions, achieved through applying different DC bias voltages, correlate well with the model prediction and thus validate the proposed model. This work, for the first time, incorporates the effect of redox level into the dynamics of conjugated polymers in an integrative way, and facilitates further analysis and control of these materials using nonlinear control tools.

© 2008 Elsevier B.V. All rights reserved.

Keywords: Conjugated polymer actuator; Polypyrrole; Redox level; Impedance model; Perturbation analysis

1. Introduction

Conjugated polymers are promising actuation materials for bio- and micro-manipulation systems, biomimetic robots, and biomedical devices [1–7]. Polypyrrole (PPy) and polyaniline are two of the most commonly used conjugated polymers for actuation purposes. The backbones of conjugated polymers have alternating single and double carbon–carbon bonds (conjugation), which results in positive charge carriers. When a sufficient positive potential is applied, electrons are removed from the polymers electrochemically (oxidation), and anions are incorporated into and/or cations are repelled out of the polymer, to maintain the charge neutrality. Application of a sufficiently negative potential can reverse the process (reduction). This reduction–oxidation (redox) process results in mass transport

of ions, which is believed to be the primary mechanism responsible for volumetric change and thus the actuation capability of conjugated polymers [5]. This can be exploited to create actuators of different configurations including, e.g., bilayer benders [1], trilayer benders [8], and linear extenders [9,10].

To achieve superior and consistent performance in applications, one needs to understand and model the complicated electro-chemo-mechanical dynamics in these materials. There has been extensive work on modeling the actuation mechanism of conjugated polymers. A physics-based “diffusive-elastic-metal” model was presented by J. Madden, where diffusion was considered to be the dominant mechanism of ions movement [11]. Geometric scaling laws for this model were recently developed by Fang et al. [12]. Christophersen et al. characterized and modeled the bending curvature for bilayer PPy microactuators of different dimensions using the beam theory [13]. Based on the single-pore model, Mao et al. proposed to capture the ion transport processes in a conjugated polymer with a finite transmission line that includes electronic resistance, ionic resistance, and double-layer capacitance [14]. In addition to physically based approaches, various phenomenological models have also been

* Corresponding author. Tel: +1 517 4325671; fax: +1 517 3531980.

E-mail addresses: fangyang@egr.msu.edu (Y. Fang),
xbtan@msu.edu (X. Tan),
gursel@uow.edu.au (G. Alici).

Nomenclature

A	PPy area (m^2)
C	double layer capacitance (F)
C^+	PPy ⁺ concentration (mol/m^3)
C^-	anion concentration (mol/m^3)
C_0	nominal anion concentration (mol/m^3)
C_1^-	perturbation of anion concentration (mol/m^3)
C_{dl}	ionic concentration in double layer (mol/m^3)
d	ionic diffusion coefficient (m^2/s)
D	electric displacement (C/m^2)
E	electric field (V/m)
F	Faraday's constant (C/mol)
h	thickness of PPy layer (m)
J	ion flux ($mol/s m^2$)
K_1	aggregate constant $dF^2/RT\kappa_e$
R	gas constant (J/mol K)
T	absolute temperature (K)
$\Delta(s)$	as defined in (23)

Greek letters

$\beta(s)$	as defined by (16)
δ	thickness of doubly layer (m)
κ_e	dielectric permittivity (F/m)
ϕ	electric potential (V)

studied. A lumped parameter model was developed by Della Santa et al. for a linear PPy actuator, which uses the model of muscle to characterize the transferred charge-induced stress [10]. Alici and coworkers investigated modeling of bending curvature and force output for trilayer PPy actuators by using finite element analysis in analogy to a thermally driven beam [15]. Samani et al. modeled the passive component of the actuator with springs and dashpots and the electro-active actuation effect through a strain generator [16].

The redox level, i.e., the amount of ions incorporated in the conjugated polymer during reduction–oxidation, has significant impact on the electromechanical properties and dynamics of the material and consequently the actuation performance. While the effect of redox level on conductivity and Young's modulus has been documented [13,17–21], its influence on dynamics of ion transport is more subtle and has received inadequate attention in terms of fundamental understanding and modeling. The latter is precisely what this paper aims to address.

In this paper a redox level-dependent impedance model is developed for conjugated polymers, which is physically based yet has a compact, explicit form. We start with a governing partial differential equation (PDE) that incorporates the dynamics of ionic diffusion, ionic migration, and redox reaction. The PDE is linearized around a given redox level via perturbation analysis, and an exact, analytical solution is obtained by converting the PDE into the Laplace domain and enforcing appropriate boundary conditions. Finally, the impedance model is derived by considering an equivalent circuit that accounts for double-layer charging, diffusion, and migration effects. While the proposed

model applies to a broad class of conjugated polymer actuators, an anion-transporting trilayer PPy actuator has been used throughout as an example.

Experiments have been conducted to verify the effectiveness of the proposed model. Different basic redox levels are established by applying a DC bias voltage of 0 V, 0.5 V, and 1 V, respectively. The impedance spectrum, from 0.08 Hz to 100 Hz, is measured by superimposing a small sinusoidal signal (amplitude 0.05 V) on the DC bias. It has been found that, while the diffusive-elastic-metal model [11] and the proposed model are comparable when the redox level is low, the latter shows clear advantage in predicting the impedance at higher redox levels.

The proposed model, for the first time, incorporates the effect of redox level into the key dynamics of conjugated polymers in an integrative way. Although it is derived under the assumption of infinitesimal perturbation, one can use it to capture the behavior under general inputs by recognizing that the redox level is in turn dictated by the impedance model. Such a feedback-type model structure opens the door to a wealth of model reduction and nonlinear control tools [22] available in the systems and control literature.

The remainder of the paper is organized as follows. In Section 2 the redox level-dependent impedance model is presented. In Section 3 experimental methods are described. Results and discussions are given in Section 4. Finally concluding remarks are provided in Section 5.

2. Model

2.1. Trilayer PPy actuator

The trilayer PPy actuator is illustrated in Fig. 1. In the middle is an amorphous, porous polyvinylidene fluoride (PVDF) layer that serves both as a backing material and a storage tank

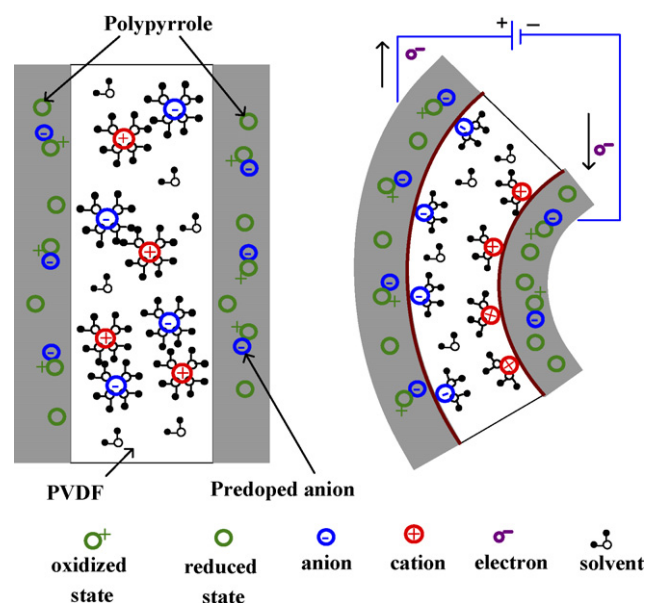


Fig. 1. Illustration of the actuation mechanism of trilayer polypyrrole actuator. Left: the sectional view of the trilayer structure; right: bending upon application of a voltage.

for the electrolyte. On both sides of the actuator are the PPy layers. When a voltage is applied across the actuator, the potential difference between the PPy layer on the anode side and the electrolyte in the PVDF layer builds up a double layer at the interface, which can be treated like a double-layer capacitance. Then the anions will be driven into and oxidize the PPy layer and cause it to expand, while the other PPy layer on the cathode side will be reduced and contract. The differential expansion thus leads to bending of the actuator, as shown in Fig. 1(right).

According to the study by Pickup [23], when conjugated polymer is reduced, it acts merely as a barrier to the migration of ions and thus can be treated as a resistor. When it is oxidized, more complicated ionic dynamics is observed. Therefore, in this paper we consider the ionic dynamics only in the oxidized PPy layer.

2.2. The governing partial differential equation

The oxidation process for an anion-transporting PPy can be represented as



Here PPy represents the neutral state of polypyrrole and PPy⁺ the oxidized state, PPy⁺A⁻ indicates that an anion A⁻ is incorporated into the polymer, and e⁻ denotes an electron. Let C⁻ and C⁺ denote the concentration of anions A⁻ and that of PPy⁺, respectively.

The anion flux **J** inside the polymer is captured by the Nernst–Planck equation [24], including both a diffusion term and an electric field-induced migration term:

$$\mathbf{J} = -d \left(\nabla C^- + \frac{C^- F}{RT} \nabla \phi \right), \quad (2)$$

where *d* is the ionic diffusion coefficient, *F* is the Faraday's constant, *R* is the gas constant, *T* is the absolute temperature, ϕ is the electric potential, and ∇ denotes the gradient. The continuity equation gives

$$\frac{\partial C^-}{\partial t} = -\nabla \cdot \mathbf{J} = d \left(\nabla \cdot \nabla C^- + \nabla \cdot \left(\frac{C^- F}{RT} \nabla \phi \right) \right), \quad (3)$$

where $\nabla \cdot$ denotes the divergence.

One can relate ϕ to the ionic concentrations through the Gauss's law:

$$\mathbf{E} = \frac{D}{\kappa_e} = -\nabla \phi \quad (4)$$

$$\nabla \cdot \mathbf{D} = F \cdot (C^+ - C^-), \quad (5)$$

where **D** denotes the electric displacement, **E** denotes the electric field, and κ_e is the dielectric permittivity of PPy.

Since the thickness of the PPy layer is much smaller than its length or width, one can assume that, inside the polymer, **J**, **D**, **E**, and other changes are all restricted to the thickness direction (denoted as *x* direction). This enables one to drop the boldface notation for these variables; in particular, *D* and *E* will be used to

represent the electric displacement and the electric field (along the *x* direction). Furthermore, (3) can be simplified as

$$\frac{\partial C^-}{\partial t} = d \left(\frac{\partial^2 C^-}{\partial x^2} + \frac{F}{RT} \frac{\partial C^-}{\partial x} \frac{\partial \phi}{\partial x} + \frac{C^- F}{RT} \frac{\partial^2 \phi}{\partial x^2} \right). \quad (6)$$

A pure delay is adopted to capture the oxidation dynamics, i.e.:

$$C^+(x, t) = C^-(x, t - T_0), \quad (7)$$

where *T*₀ is the time taken for an anion A⁻ to react with PPy. Finally, there are two boundary conditions for (6): (1) C⁻ at *x* = 0 equals the concentration in the PPy/PVDF double layer; (2) the ionic flux *J*(*x*, *t*) at *x* = *h* (the other boundary of PPy layer) vanishes, assuming no ions leaking outside.

Eqs. (4)–(7), and the boundary conditions form a complete description of the ionic dynamics inside PPy.

2.3. Perturbation analysis

From (4) and (5), one can express ($\partial\phi/\partial x$) and ($\partial^2\phi/\partial x^2$) as

$$\frac{\partial \phi}{\partial x} = -\frac{F}{\kappa_e} \int_0^x (C^+ - C^-) d\xi + \frac{\partial \phi}{\partial x}(0, t) \quad (8)$$

$$\frac{\partial^2 \phi}{\partial x^2} = -\frac{F}{\kappa_e} (C^+ - C^-). \quad (9)$$

Supposing that the double layer charging process is relatively fast comparing to the ionic dynamics in PPy (which is usually the case), the net charge inside the double layer is zero. Further assume that the electrolyte in PVDF has good ionic conductivity, and thus the electric field within is negligible. Under these assumptions, one can apply Gauss's law to a small volume containing the double layer and conclude ($\partial\phi/\partial x$)(0, *t*) = 0 in (8). Plugging (8), (9), and (7) into (6), one obtains

$$\begin{aligned} \frac{\partial C^-}{\partial t} = d \left(\frac{\partial^2 C^-}{\partial x^2} - \frac{F^2}{RT\kappa_e} C^- (C^-(x, t - T_0) - C^-(x, t)) \right. \\ \left. - \frac{F^2}{RT\kappa_e} \frac{\partial C^-}{\partial x} \int_0^x (C^-(\xi, t - T_0) - C^-(\xi, t)) d\xi \right). \end{aligned} \quad (10)$$

Eq. (10) is a nonlinear integro-differential equation that cannot be solved analytically. We introduce perturbation analysis to linearize it around a nominal concentration *C*₀, which represents the redox level of the conjugated polymer. To proceed, let

$$C^-(x, t) = C_0 + \varepsilon C_1^-(x, t), \quad (11)$$

with 0 < ε ≪ 1. In (11), $\varepsilon C_1^-(x, t)$ represents the small perturbation imposed on *C*₀. Plugging (11) into (10) and neglecting terms involving ε^2 , one gets the following linearized equation that depends on the redox level *C*₀:

$$\frac{\partial C_1^-}{\partial t} = d \left(\frac{\partial^2 C_1^-}{\partial x^2} - \frac{F^2}{RT\kappa_e} C_0 (C_1^-(x, t - T_0) - C_1^-(x, t)) \right). \quad (12)$$

To obtain an analytical solution, one can convert (12) from the time domain to the Laplace domain:

$$sC_1^- = d \left(\frac{\partial^2 C_1^-}{\partial x^2} + \frac{F^2 C_0}{RT\kappa_e} \cdot (1 - e^{-sT_0}) C_1^- \right), \quad (13)$$

where s is the Laplace variable.

Eq. (13) can be further written as

$$\frac{\partial^2 C_1^-}{\partial x^2} = \frac{s - K_1 C_0 (1 - e^{-sT_0})}{d} C_1^-, \quad (14)$$

with the constant

$$K_1 \triangleq \frac{dF^2}{RT\kappa_e}.$$

The solution of (14) has a generic form

$$C_1^-(x, s) = \alpha_1(s) e^{\beta(s)x} + \alpha_2(s) e^{-\beta(s)x}, \quad (15)$$

with

$$\beta(s) = \sqrt{\frac{s - K_1 C_0 (1 - e^{-sT_0})}{d}}. \quad (16)$$

The functions $\alpha_1(s)$ and $\alpha_2(s)$ are determined by the boundary conditions. The boundary condition at the PPy/PVDF interface, $x = 0$, is

$$C_1^-(0, s) = C_{dl}(s), \quad (17)$$

where $C_{dl}(s)$ denotes the ionic concentration in the double layer. Combining (15) and (17) gives

$$\alpha_1(s) + \alpha_2(s) = C_{dl}(s). \quad (18)$$

The other boundary condition, at $x = h$, requires that the ionic flux be zero. Using (2), (8), and (11), and ignoring terms involving ε^2 , the zero flux condition at $x = h$ reads

$$\frac{\partial C_1^-}{\partial x}(h, s) + \frac{C_0 F^2}{RT\kappa_e} (1 - e^{-sT_0}) \int_0^h C_1^-(\xi, s) d\xi = 0. \quad (19)$$

Plugging (15) into (19), one gets

$$s(\alpha_1(s) e^{\beta(s)h} - \alpha_2(s) e^{-\beta(s)h}) = (s - d\beta^2(s))(\alpha_1(s) - \alpha_2(s)). \quad (20)$$

Combining (18) and (20), one can solve for α_1 and α_2 :

$$\alpha_1(s) = \frac{s e^{-\beta(s)h} - (s - d\beta^2(s))}{\Delta(s)} C_{dl}(s), \quad (21)$$

$$\alpha_2(s) = \frac{s e^{\beta(s)h} - (s - d\beta^2(s))}{\Delta(s)} C_{dl}(s). \quad (22)$$

with $\Delta(s)$ defined as

$$\Delta(s) = s(e^{\beta(s)h} + e^{-\beta(s)h}) - 2(s - d\beta^2(s)). \quad (23)$$

2.4. Impedance model

Fig. 2 shows the equivalent circuit for the proposed impedance model. The total current I consists of three components, the double layer charging current I_C , the diffusion current

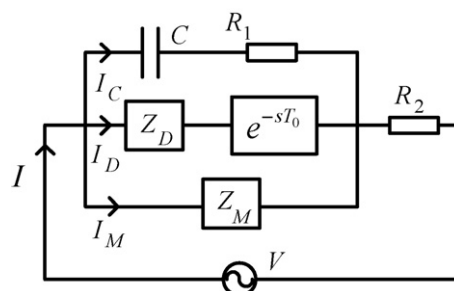


Fig. 2. Equivalent circuit for the impedance model.

I_D , and the migration current I_M . In the figure C denotes the double layer capacitance, R_1 is the ohmic resistance of the oxidized PPy layer, and R_2 denotes the resistance of the reduced PPy layer, the PVDF (electrolyte) layer, and the contacts. Z_D and Z_M represent the diffusion dynamics and the migration dynamics, respectively. Each of the current components is discussed next. We will be concerned with the voltage/current associated with the charge concentration perturbation εC_1^- .

2.4.1. Double layer charging current I_C

Double-layer charges are established at the PPy/PVDF interface in response to an applied voltage, which can be captured equivalently through a double layer capacitance C . The total stored charge in the double layer is $\varepsilon F A \delta C_{dl}(s)$, where A and δ denote the area of PPy layer and the thickness of the double layer, respectively. The time derivative of the stored charge gives I_C :

$$I_C(s) = \varepsilon F A \delta s C_{dl}(s). \quad (24)$$

2.4.2. Diffusion current I_D

The diffusion flux at the PPy/PVDF interface (i.e., $x = 0$) is given by the Fick's law and equals $-d\varepsilon(\partial C_1^- / \partial x)(0, s)$. But an electron is not released until the oxidation takes place after T_0 delay. I_D is thus expressed as

$$I_D(s) = -\varepsilon F A d e^{-sT_0} \frac{\partial C_1^-}{\partial x}(0, s) = -\varepsilon F A d e^{-sT_0} \beta(s)(\alpha_1(s) - \alpha_2(s)) \quad (25)$$

$$= \frac{\varepsilon F A d s e^{-sT_0} \beta(s)(e^{\beta(s)h} - e^{-\beta(s)h})}{\Delta(s)} C_{dl}(s), \quad (26)$$

where the second equality follows from (15).

2.4.3. Migration current I_M

I_M is induced by the net charges Q_P inside the PPy layer. Applying the integral form of Gauss's law to the PPy layer and recalling $E(0, s) = 0$, one can obtain

$$Q_P(s) = A D(h, s) = A \kappa_e E(h, s) = -A \kappa_e \frac{\partial \phi}{\partial x}(h, s) = -\varepsilon F A (1 - e^{-sT_0}) \int_0^h C_1^-(\xi, s) d\xi \quad (27)$$

$$= -\varepsilon FA(1 - e^{-sT_0}) \frac{\alpha_1 e^{\beta h} - \alpha_2 e^{-\beta h} - (\alpha_1 - \alpha_2)}{\beta}, \quad (28)$$

where (27) follows from (8) and (28) follows from (15). I_M is then expressed as

$$\begin{aligned} I_M(s) &= sQ_P(s) \\ &= -\varepsilon FAs(1 - e^{-sT_0}) \frac{\alpha_1 e^{\beta h} - \alpha_2 e^{-\beta h} - (\alpha_1 - \alpha_2)}{\beta} \\ &= -\frac{\varepsilon FAd s(1 - e^{-sT_0})\beta(s)(e^{\beta(s)h} - e^{-\beta(s)h})}{\Delta(s)} C_{dl}(s). \end{aligned} \quad (29)$$

Since the total current is

$$I(s) = I_C(s) + I_D(s) + I_M(s), \quad (30)$$

and the total potential drop (see Fig. 2) is

$$V(s) = \frac{I_C(s)}{sC} + R_1 I_C(s) + R_2 I(s), \quad (31)$$

the impedance of the trilayer conjugated polymer actuator can be calculated using (24), (26), and (29):

$$\begin{aligned} Z(s) &= \frac{V(s)}{I(s)} = R_2 \\ &+ \frac{\delta\Delta(s)(1 + sR_1C)}{sC(\delta\Delta(s) + d\beta(s)(2e^{-sT_0} - 1)(e^{\beta(s)h} - e^{-\beta(s)h}))}. \end{aligned} \quad (32)$$

The model captures the dependence on the redox level C_0 through $\beta(s)$ defined in (16). The model is consistent with the diffusive-elastic-metal model [11,12] when the migration dynamics and the oxidation dynamics are ignored.

3. Materials and experiments

3.1. Materials

The trilayer PPy actuator is fabricated by the Intelligent Polymer Research Institute at the University of Wollongong, Australia, and a description of the fabrication process can be found in, e.g., [25]. The PVDF layer is 110 μm thick, while each PPy layer is 30 μm thick. The electrolyte used is tetrabutylammonium hexafluorophosphate ($\text{TBA}^+\text{PF}_6^-$) in the solvent propylene carbonate (PC), where PF_6^- is the mobile anions that can transfer into and out of the PPy layer. Each actuator is soaked in the electrolyte before testing for 2 h. The electrolyte stored in the PVDF layer enables the actuator to work in air for several hours. Notice that both PPy layers were already doped with certain PF_6^- during fabrication.

3.2. Experiments

A computer equipped with a DS1104 R&D Controller Board (dSPACE Inc.) is used for data acquisition and processing. A trilayer actuator is clamped on one end, where electrical contacts are made using copper tapes coated with silver. The applied actuation voltage and the corresponding current are measured.

Table 1
Estimated values for C and R_1

Parameter	Samples 1–3	Samples 4–6
C (F)	1.03×10^{-4}	3.17×10^{-4}
R_1 (Ω)	2×10^{-5}	8.3×10^{-6}

All the experiments were conducted at temperatures between 22 °C and 24 °C.

The samples were predoped with PF_6^- during fabrication, and the nominal concentration C_0 in the absence of DC bias is estimated to be 1000 mol/m³ based on the deposition conditions. Different C_0 is obtained by applying DC biases of 0.5 V and 1 V, respectively, where the change in C_0 is calculated by dividing the transferred charges before reaching the steady state by the PPy volume. Sinusoidal voltages of amplitude 0.05 V and frequency 0.08–200 Hz are superimposed on the DC voltage, as perturbations, for the measurement of impedance spectrum. Electrolyte is prepared for two concentrations, 0.35 M and 0.25 M, for two sets of experiments. In each set, three samples of same dimensions and from the same fabrication batch are prepared and subject to DC voltages of 0 V, 0.5 V, and 1 V, respectively. The samples prepared with 0.35 M electrolyte have dimensions 15 mm \times 5 mm, while those with 0.25 M electrolyte have dimensions 30 mm \times 6 mm. For the convenience of referencing, the samples with 0.35 M electrolyte are named Sample 1 (0 V), Sample 2 (0.5 V) and Sample 3 (1 V). The samples with 0.25 M electrolyte are named Samples 4–6 in the same manner.

4. Results and discussions

4.1. Estimation of model parameters

Some parameters of the model (32) are physical constants or can be measured directly, including gas constant $R = 8.3143$ J/mol K, Faraday's constant $F = 96487$ C/mol, absolute temperature $T = 300$ K, and PPy thickness $h = 3 \times 10^{-5}$ m.

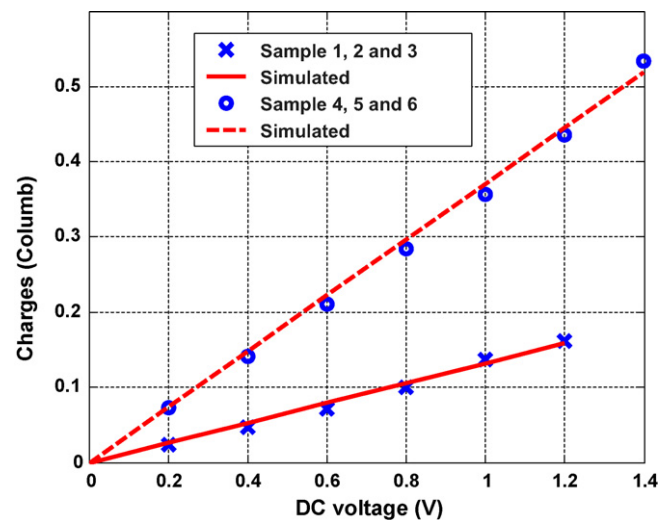


Fig. 3. The relationship between transferred charges and applied voltage for different samples.

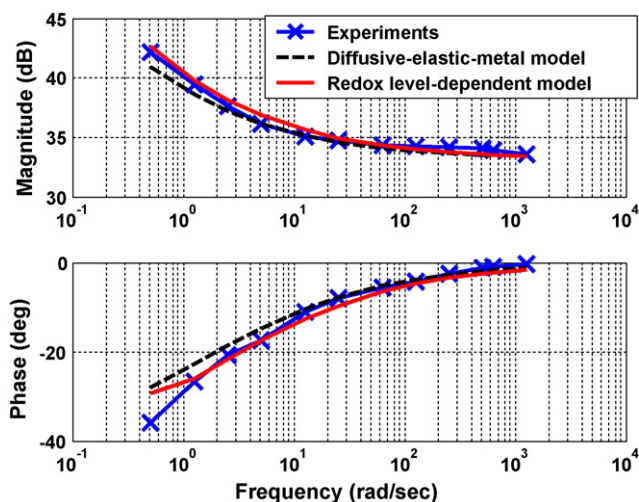


Fig. 4. Model predictions vs. experimental impedance for Sample 1 (0.35 M electrolyte, 0 V DC voltage).

Based on studies on the dielectric properties of conjugated polymers [26–28], the dielectric permittivity κ_e is taken to be $60\epsilon_0$, where ϵ_0 represents the permittivity in vacuum. The double layer thickness δ is difficult to measure, and an estimation of 25 nm is used based on the range reported in [29].

Experiments are conducted to estimate the double-layer capacitance C , the nominal redox level C_0 , and the resistances R_1 and R_2 . If we assume that the internal capacitance of the polymer per unit volume is close to the double-layer capacitance per unit volume [11], C can be estimated using

$$C = \frac{Q}{U} \cdot \frac{\delta}{h}, \quad (33)$$

where Q is the charge transferred under an applied DC voltage U . Fig. 3 shows the transferred charges under DC voltages from 0.2 V to 1.2 V for different samples, from which Q/U is estimated to be 0.13 for Samples 1, 2, 3, and 0.37 for Samples 4–6. Estimated values of C based on (33) are listed in Table 1. Also listed in the table are the values for the resistance R_1 , which are estimated

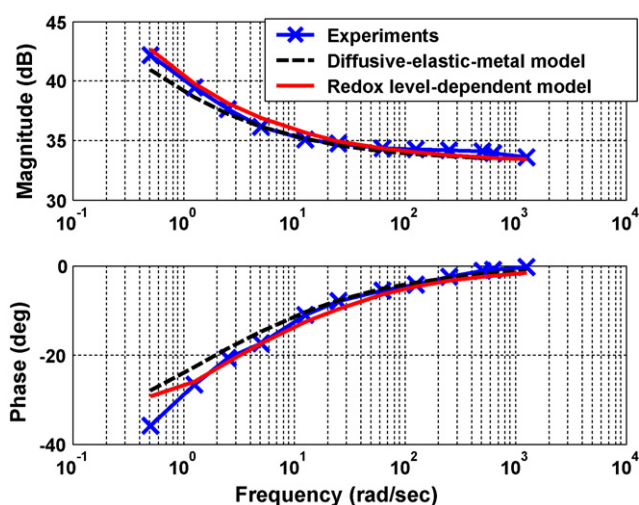


Fig. 5. Model predictions vs. experimental impedance for Sample 2 (0.35 M electrolyte, 0.5 V DC voltage).

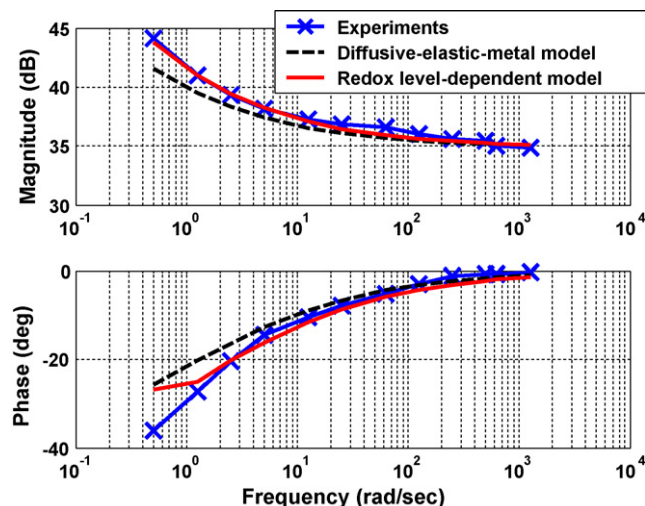


Fig. 6. Model predictions vs. experimental impedance for Sample 3 (0.35 M electrolyte, 1 V DC voltage).

with a conductivity of 200 S/cm based on the studies on PPy doped with PF_6^- [30,31] under room pressure and temperature. The results in Fig. 3, together with the sample dimensions, also enables us to compute the nominal anion concentrations (redox level) C_0 , which are listed in Table 2. Finally, to measure R_2 , a sinusoidal input $0.05 \sin(500\pi t)$ V is applied. Note that the small amplitude ensures minimal influence on C_0 . At this high frequency, the trilayer actuator is almost resistive and the measured impedance is approximately $R_1 + R_2$. It is observed that R_1 is negligible compared with the measured resistance, thus R_2 is chosen to be the measured resistance. Since the redox level has impact on the resistance of the reduced PPy layer, values of R_2 will be different for different samples, as shown in Table 2.

The only remaining parameters are the diffusion constant d and the time delay of oxidation T_0 , which will be identified through curve fitting, to be described in the next subsection.

4.2. Model verification

Experimentally measured impedance spectra have been used to verify the proposed redox level-dependent impedance model. For comparison purposes, the diffusive-elastic-metal model [11] has also been used. Besides the parameters estimated in the previous subsection, the only free parameter for the diffusive-elastic-metal model is the diffusion constant d . For each set of experiments (0.35 M or 0.25 M electrolyte), the value of d is estimated by fitting the diffusive-elastic-metal model to the mea-

Table 2
Estimated values for C_0 and R_2

	C_0 (mol/m ³)	R_2 (Ω)
Sample 1	1000	34.0
Sample 2	1323	46.3
Sample 3	1646	56.7
Sample 4	1000	26.6
Sample 5	1363	30.2
Sample 6	1726	50.3

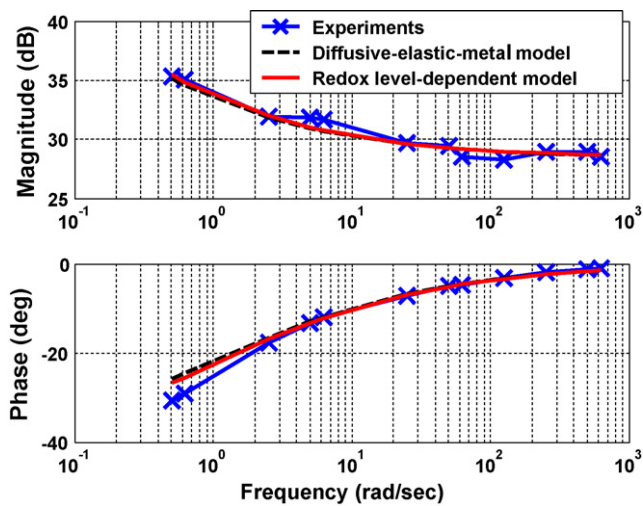


Fig. 7. Model predictions vs. experimental impedance for Sample 4 (0.25 M electrolyte, 0 V DC voltage).

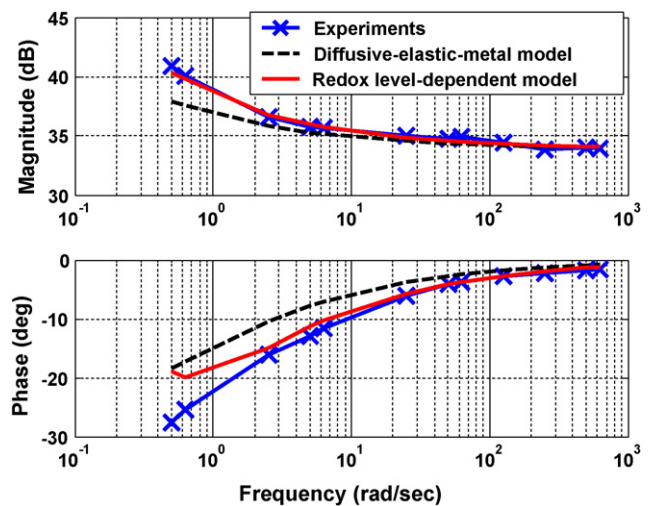


Fig. 9. Model predictions vs. experimental impedance for Sample 6 (0.25 M electrolyte, 1 V DC voltage).

sured impedance spectrum under a DC voltage of 0 V. The same value will be used for the proposed model as well. The last parameter, T_0 , for the proposed model, is obtained by fitting the measured impedance spectrum under a DC bias of 0.5 V. Then the measured spectra under DC voltages of 0 V and 1 V are compared to the predictions by the redox level-dependent model, without further tuning of any parameters, thus serving as independent checks on the proposed model. Note that the predictions by the diffusive-elastic-metal model do not vary with the DC bias.

Figs. 4–6 show the results for Sample 1 through Sample 3. Using the aforementioned methods, the values of d and T_0 are identified as: $d = 2.5 \times 10^{-11} \text{ m}^2/\text{s}$, $T_0 = 1.9 \text{ ns}$. It is found that, while the two models are comparable at a low redox level, the proposed model shows clear advantage at higher redox levels, as can be seen in Figs. 5 and 6. Consistent results are obtained for Samples 4–6. Here d and T_0 are estimated to be $d = 1.5 \times 10^{-11} \text{ m}^2/\text{s}$, $T_0 = 4 \text{ ns}$. It is again seen that the proposed model is

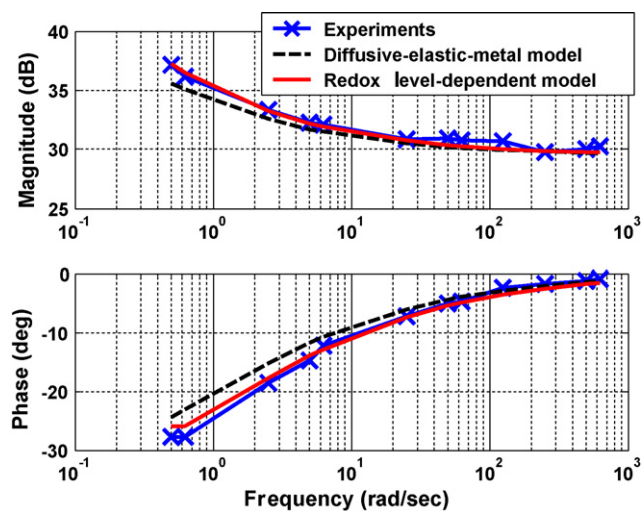


Fig. 8. Model predictions vs. experimental impedance for Sample 5 (0.25 M electrolyte, 0.5 V DC voltage).

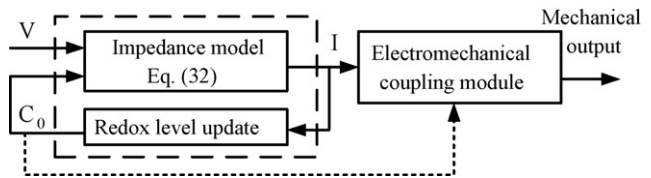


Fig. 10. A feedback connection perspective capturing the redox level-dependent electrodynamics for general inputs.

able to capture the redox-level-dependent impedance, as shown in Figs. 7–9.

4.3. Discussion on the model

Although the redox level-dependent impedance model was derived using perturbation analysis, it can be used to describe the electrochemical dynamics for a much broader class of inputs instead of being restricted to small input signals. This will be achieved by a feedback connection of the proposed model with a module that translates the current (and thus the transferred charge) to the redox level, as illustrated in Fig. 10. In other words, the output of the redox level-dependent impedance model can be used to update the redox level parameter C_0 . The electromechanical coupling module relates the mechanical output of the actuator to the transferred charge, as discussed in [11,12]. Note that the redox level could also influence the parameters of the electromechanical module, an example of which is the Young's modulus. The perspective presented in Fig. 10 will enable the use of model reduction, nonlinear analysis and control tools [22] in dealing with the sophisticated behavior of conjugated polymer actuators.

5. Conclusions

In this paper a redox level-dependent impedance model was proposed for conjugated polymer actuators. The model was derived based on a nonlinear partial differential equation that incorporates the dynamics of ion diffusion, ion migration, and

polymer oxidation, which was linearized using perturbation techniques. The linearized PDE was solved analytically in the Laplace domain, with proper boundary conditions enforced. Comparison with experimental results supported that the proposed model is able to capture the influence of redox level on the impedance spectrum. The model provides an effective way to integrate the diffusion and migration effects of ion flux in conjugated polymers, which used to be treated separately with different models [32,14].

The proposed model not only contributes to fundamental understanding of the complicated, redox level-dependent electrochemical behavior, but also holds potential for nonlinear control of conjugated polymer actuators. In particular, the feedback connection between the model and the module updating the redox level can significantly extend the applicable regime for the model. Work is currently underway to investigate control strategies for the nonlinear feedback model.

Acknowledgements

This research was supported in part by an NSF CAREER grant (ECS 0547131) and MSU IRGP (05-IRGP-418).

References

- [1] E. Smela, O. Inghanas, I. Lundstrom, Controlled folding of micro-size structures, *Science* 268 (1995) 1735–1738.
- [2] E.W.H. Jager, O. Inghanas, I. Lunnstrom, Microrobots for micrometer-size objects in aqueous media: potential tools for single cell manipulation, *Science* 288 (2000) 2335–2338.
- [3] J. Zhou, H. Chan, T. To, K. Lai, W.J. Li, Polymer MEMS actuators for underwater micromanipulation, *IEEE/ASME Trans. Mech.* 9 (2) (2004) 334–342.
- [4] Y. Bar-Cohen (Ed.), *Electroactive Polymer (EAP) Actuators as Artificial Muscles: Reality, Potential, and Challenges*, SPIE–The International Society for Optical Engineering, Bellingham, WA, 2001.
- [5] E. Smela, Conjugated polymer actuators for biomedical applications, *J. Adv. Mater.* 15 (6) (2003) 481–494.
- [6] F. Carpi, D. De Rossi, Electroactive polymer-based devices for e-textiles in biomedicine, *IEEE Trans. Informat. Technol. Biomed.* 9 (3) (2005) 295–318.
- [7] C. Immerstrand, K.H. Peterson, K.-E. Magnusson, E.W.H. Jager, M. Krogh, M. Skoglund, A. Selbing, O. Inghanas, Conjugated-polymer micro- and milliactuators for biological applications, *Mater. Res. Soc. Bull.* 27 (6) (2002) 461–464.
- [8] G. Alici, B. Mui, C. Cook, Bending modeling and its experimental verification for conducting polymer actuators dedicated to manipulation applications, *Sens. Actuators A* 126 (2006) 396–404.
- [9] R. Baughman, Conducting polymer artificial muscles, *Synth. Met.* 78 (1996) 339–353.
- [10] A. Della Santa, D. De Rossi, A. Mazzoldi, Characterization and modelling of a conducting polymer muscle-like linear actuator, *Smart Mater. Struct.* 6 (1997) 23–34.
- [11] J.D.W. Madden, *Conducting polymer actuators*, PhD thesis, MIT, 2000.
- [12] Y. Fang, X. Tan, Y. Shen, N. Xi, G. Alici, A scalable model for trilayer conjugated polymer actuators and its experimental validation, *Mater. Sci. Eng. C: Bio. Supramol. Syst.* 28 (2008) 421–428.
- [13] M. Christophersen, B. Shapiro, E. Smela, Characterization and modeling of PPy bilayer microactuators. Part 1. Curvature, *Sens. Actuators B* 115 (2006) 596–609.
- [14] H. Mao, J. Ochmanska, C. Paulse, P. Pickup, Ion transport in pyrrole-based polymer films, *Faraday Dis. Chem. Soc.* 88 (1989) 165–176.
- [15] P. Metz, G. Alici, G. Spinks, A finite element model for bending behaviour of conducting polymer electromechanical actuators, *Sens. Actuators A* 130–131 (2006) 1–11.
- [16] M. Samani, P. Whitten, G. Spinks, C. Cook, Modelling of polypyrrole actuators, *Mater. Res. Soc. Proc.* 889 (2005) W03–W05.
- [17] T. Skotheim, J. Reynolds, *Conjugated Polymers: Processing and Applications*, 3rd ed., CRC Press, 2006.
- [18] D.L. Boxall, R.A. Osteryoung, Switching potentials and conductivity of polypyrrole films prepared in the ionic liquid 1-butyl-3-methylimidazolium hexafluorophosphate, *J. Electrochem. Soc.* 151 (2) (2004) E41–E45.
- [19] H. Mao, P. Pickup, In situ measurement of the conductivity of polypyrrole and poly[1-methyl-3-(pyrrol-1-ylmethyl)pyridinium]⁺ as a function of potential by mediated voltammetry redox conduction or electronic conduction? *J. Am. Chem. Soc.* 112 (1990) 1776–1782.
- [20] G. Spinks, L. Liu, G. Wallace, D. Zhou, Strain response from polypyrrole actuators under load, *Adv. Funct. Mater.* 12 (2002) 437–440.
- [21] D. De Rossi, A. Della Santa, A. Mazzoldi, Performance and work capacity of a polypyrrole conducting polymer linear actuator, *Synth. Met.* 90 (1997) 93–100.
- [22] H.K. Khalil, *Nonlinear Systems*, 3rd ed., Prentice Hall, 2002.
- [23] P. Pickup, Alternating current impedance study of a polypyrrole-based anion-exchange polymer, *J. Chem. Soc., Faraday Trans.* 86 (1990) 3631–3636.
- [24] N. Lakshminarayanaiah, *Transport Phenomena in Membranes*, Academic Press, 1969.
- [25] Y. Wu, G. Alici, G.M. Spinks, G.G. Wallace, Fast trilayer polypyrrole bending actuators for high speed applications, *Synth. Met.* 156 (2006) 1017–1022.
- [26] G. Phillips, R. Suresh, J. Waldman, J. Kumar, J. I-Chen, S. Tripathy, J. Huang, Dielectric property of polypyrrole doped with tosylate anion in the far infrared and microwave, *J. Appl. Phys.* 69 (1991) 899–905.
- [27] F. Legros, A. Fourrier-Lamer, Dielectric property of doped polypyrrole in the 5 Hz–1 GHz frequency range, *Mater. Res. Bull.* 19 (1984) 1109–1117.
- [28] S. Saafan, M. El-Nimr, E. El-Ghazzawy, Study of dielectric properties of polypyrrole prepared using two different oxidizing agents, *J. Appl. Polym. Sci.* 99 (2006) 3370–3379.
- [29] S. Satyanarayana, Surface stress and capacitive MEMS sensor arrays for chemical and biological sensing, PhD thesis, University of California, Berkeley, 2005.
- [30] C.O. Yoon, M. Reghu, D. Moses, A.J. Heeger, Transport near the metal-insulator transition: polypyrrole doped with PF₆⁻, *Phys. Rev. B (Condensed Matter)* 49 (1994) 10851–10863.
- [31] B. Chapman, R. Buckley, N. Kemp, A. Kaiser, D. Beaglehole, H. Trodahl, Low-energy conductivity of PF₆⁻-doped polypyrrole, *Phys. Rev. B (Condensed Matter)* 60 (1999) 13479–13483.
- [32] C. Ho, I. Raistrick, R. Huggins, Application of a-c techniques to the study of lithium diffusion in tungsten trioxide thin films, *J. Electrochem. Soc.* 127 (1980) 343–350.

Biographies

Yang Fang received the Bachelor's degree in Automatic Control from University of Science and Technology of China, in 2003, and Master's degree in Manufacturing System and Technology from Nanyang Technological University, Singapore, in 2005. Since 2005 he has been working towards his PhD degree in the Electrical and Computer Engineering Department, Michigan State University, USA. His PhD thesis is focused on the modeling and control of conjugated polymer actuators, modeling of conjugated polymer sensors, and bio/micro applications of these materials.

Xiaobo Tan received the Bachelor's and Master's degrees in Automatic Control from Tsinghua University, Beijing, China, in 1995, 1998, and his PhD in Electrical and Computer Engineering from the University of Maryland at College Park, USA, in 2002. From September 2002 to July 2004 he was a Research Associate with the Institute for Systems Research at the University of Maryland. In August 2004 he joined the Department of Electrical and Computer Engineering at Michigan State University as an Assistant Professor. His research interests include electroactive polymer sensors and actuators, modeling and control of

smart materials, biomimetic robotics, bio/micro-manipulation, and collaborative control of unmanned vehicles. Dr. Tan was a recipient of the NSF CAREER Award in 2006.

Gursel Alici received the PhD degree in Robotics from the Department of Engineering Science, Oxford University, UK, in 1993. He is currently an Associate Professor of Mechatronic Engineering at the University of Wollon-

gong, NSW, Australia, where he leads Mechatronic Engineering. His current research interests include intelligent mechatronic systems involving mechanisms/serial/parallel robot manipulators, micro/nano manipulation systems, and modeling, analysis, characterization, control and micro/nano fabrication of conducting polymer actuators and sensors for robotic and biomimetic applications.